Electronic Supplementary Information

for

A Conductive Vanadium-Porphyrinic MOF as an Exclusive Durable Electrode for Efficient Oxygen Evolution

Soumen Khan,[a,b] Anirban Biswas,[a] Santanu Chand,*[,c] and Chanchal Chakraborty*[,a,b]

[a] *Department of Chemistry, Birla Institute of Technology & Science (BITS) Pilani, Hyderabad Campus. Jawaharnagar, Samirpet, Hyderabad, Telangana 500078, India.*

E-mail: chanchal@hyderabad.bits-pilani.ac.in (Dr. Chanchal Chakraborty)

[b] *Materials Center for Sustainable Energy & Environment (McSEE), Birla Institute of Technology & Science (BITS) Pilani, Hyderabad Campus. Jawaharnagar, Samirpet, Hyderabad, Telangana 500078, India.*

[c] *Institute of Nanoscience & Technology (INST), Mohali, Sector 81, Sahibzada Ajit Singh Nagar, Punjab 140306, India*

Email: santanuchand@inst.ac.in ; chand2santanu@gmail.com (Dr. Santanu Chand)

1. Materials and Synthesis:

1.1. materials: Commercial chemicals were used as received unless otherwise stated. Vanadium (III) chloride (VCl_3, 98%), N, N-dimethylformamide (DMF, 99%), anhydrous methanol (MeOH, 99%), acetone (99%), and tetrakis(4-carboxyphenyl)porphyrin were purchased from Sigma-Aldrich Corporation and Tokyo Chemical Industry (India) Pvt. Ltd. All chemicals were used without further purification. Water used was double-distilled and Millipore water. Pyridine (Py), N-methyl pyrrolidone (NMP, ACS grade, Fisher Scientific), methanol (MeOH, HPLC grade, Fisher Scientific), KOH, Nafion, and commercial Activated Carbon (AC) were purchased from commercial sources. The KOH aqueous solution used for the electrochemical studies was prepared using deionised water. Ni-foam (thickness ≤ 2.5 mm) was purchased from GRS Corporation, India. Solvothermal syntheses were conducted in a round-bottom flask**.**

1.2. Synthetic procedures of V-MOF:

A one-pot mixture containing VCl_3 and tetrakis(4-carboxyphenyl)porphyrin in DMF was solvothermally reacted at 150 ˚C for 24 h to yield a dark red-brown microcrystalline product, termed V-MOF. The microcrystalline V-MOF-10 was then washed with DMF before any further analyses to remove the unreacted materials. The obtained product was subsequently exchanged with MeOH and acetone, respectively, and activated at 150 ˚C for 24 h under a dynamic vacuum to remove the guest molecules within the pores.[S1]

2. Experimental section

2. 1. General Physicochemical Characterisation Tools: Powder X-ray diffraction (PXRD) patterns were recorded on a Rigaku Ultima IV diffractometer using Cu Kα radiation (λ = 1.54 Å). Data were collected over a 2θ range of 5–40°, with a step size of 0.01° and a scanning rate of 1° min^{-1}, under identical conditions for all samples. UV–vis spectra were obtained using a JASCO V-670 spectrometer. Morphological characterisation and energy-dispersive X-ray (EDX) analysis of Ni-NS were performed by field emission scanning electron microscopy (FE-SEM). Samples were prepared by drop-casting the material onto a silicon wafer and air-drying at room temperature. Imaging was performed on a FEI Apreo LoVac microscope operating at 20 kV. High-resolution transmission electron microscopy (HRTEM) was conducted on a FEI Tecnai G2 S-Twin microscope with an accelerating voltage of 200 kV. Nitrogen adsorption-desorption isotherms were measured at 77 K using a Microtrac Bel BELSORP-mini II surface area analyser, following activation of the crystals at 90 °C under vacuum for 24 h. The

Brunauer-Emmett-Teller (BET) surface area and pore size distribution were derived from the adsorption data. X-ray photoelectron spectroscopy (XPS) was performed on a Thermo Scientific K-Alpha system equipped with an Al Kα source (1486.8 eV). Thermogravimetric analysis (TGA) of Ni-NS was carried out using a Shimadzu DTG-60 instrument from 30 to 800 °C at a heating rate of 10 °C min^{-1} under a nitrogen atmosphere. OER measurements were conducted using an Autolab PGSTAT128N Potentiostat.

2.2. Electrochemical Characterisations: Electrochemical studies were carried out using a three-electrode configuration, where a V-MOF (activated at 100 ^{O}C overnight in a vacuum oven) modified Ni foam (1.0 × 1 cm^2) served as the working electrode (WE), a platinum wire as the counter electrode (CE), and Ag/AgCl (saturated KCl) as the reference electrode (RE). Linear sweep voltammetry (LSV) and CV were used to investigate the electrocatalytic behaviour in a 1 M KOH solution, with LSV over 0 to 1.2 V at a scan rate of 10 mV s_{-1}. Cyclic voltammetry (CV) was performed in the potential window of 0-0.1 V, to calculate the ECSA. Electrochemical impedance spectroscopy (EIS) was recorded in the frequency range of 0.01 Hz to 10 kHz with an AC perturbation.

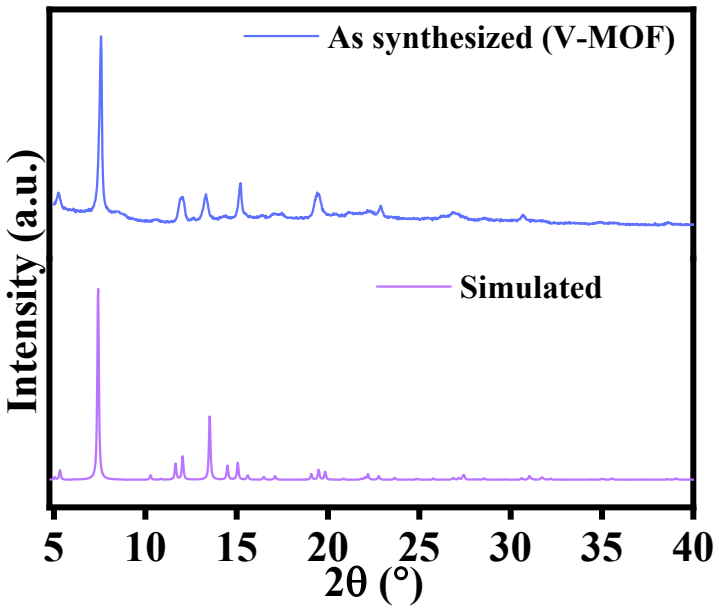

Fig. S1. Simulated PXRD pattern with as-synthesised V-MOF.

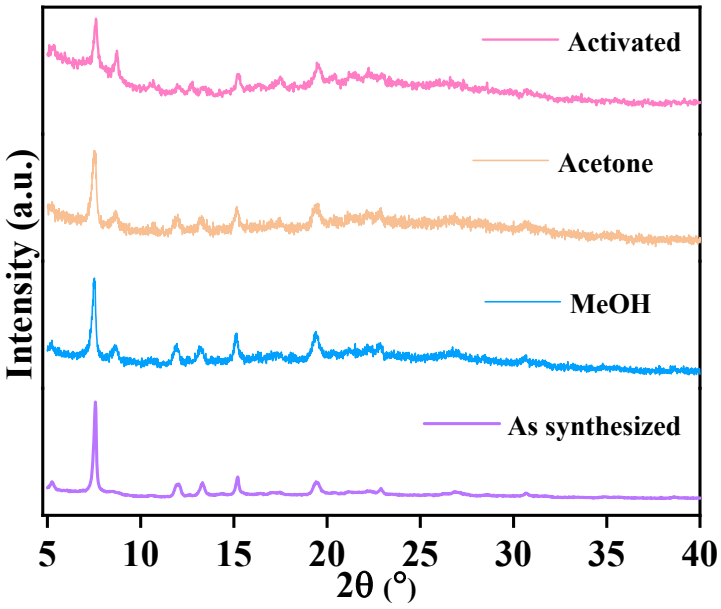

Fig. S2. PXRD patterns of as-synthesised V-MOF after exchange in methanol and acetone, and after activation at 100 °C under vacuum overnight.

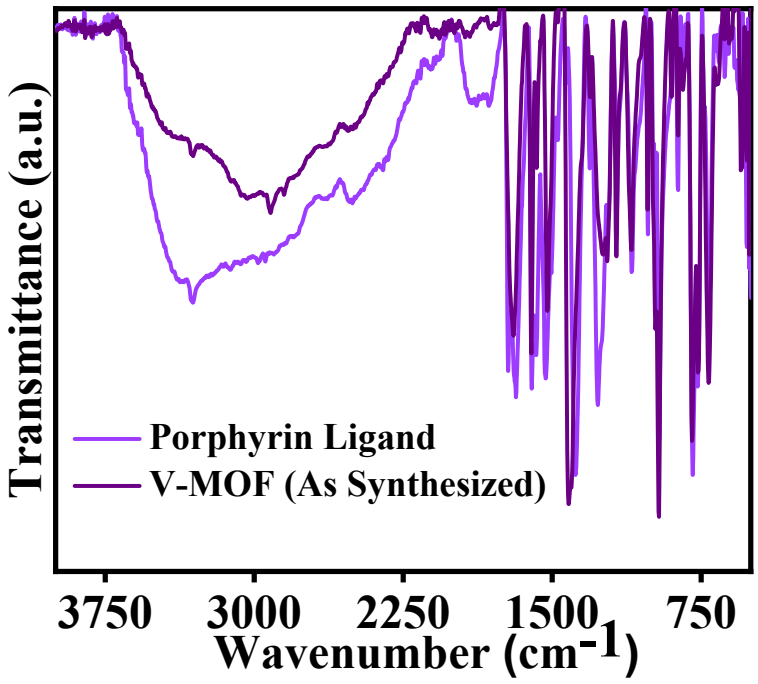

Fig. S3. FT-IR spectroscopy of the Porphyrin ligand and corresponding porphyrin-based V-MOF.

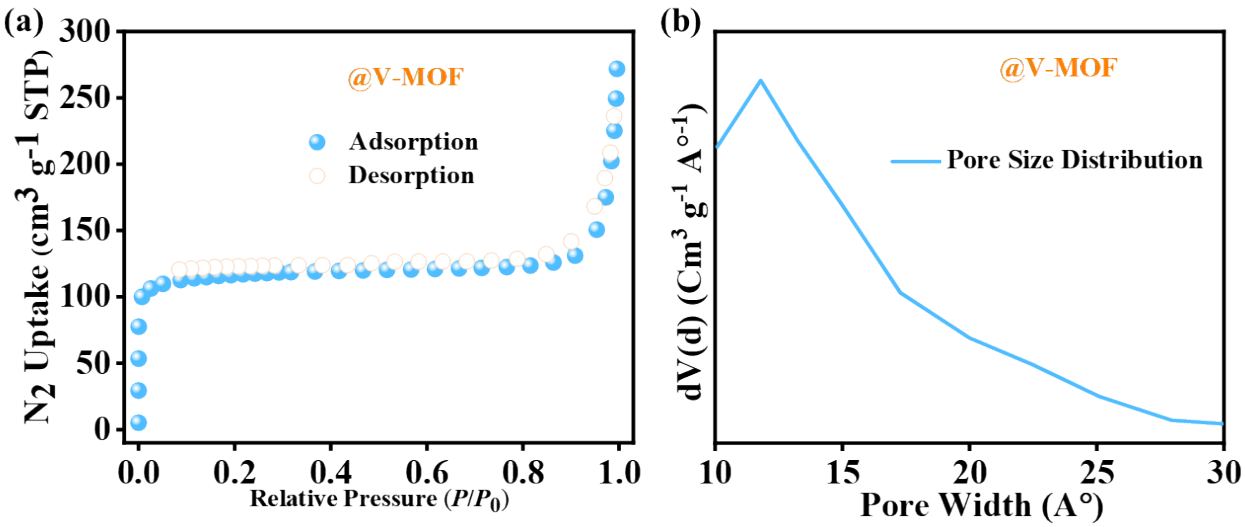

Fig. S4. (a) The N_2 adsorption measurement at 77 K shows the BET surface area of V-MOF; (b) the pore size distribution of V-MOF.

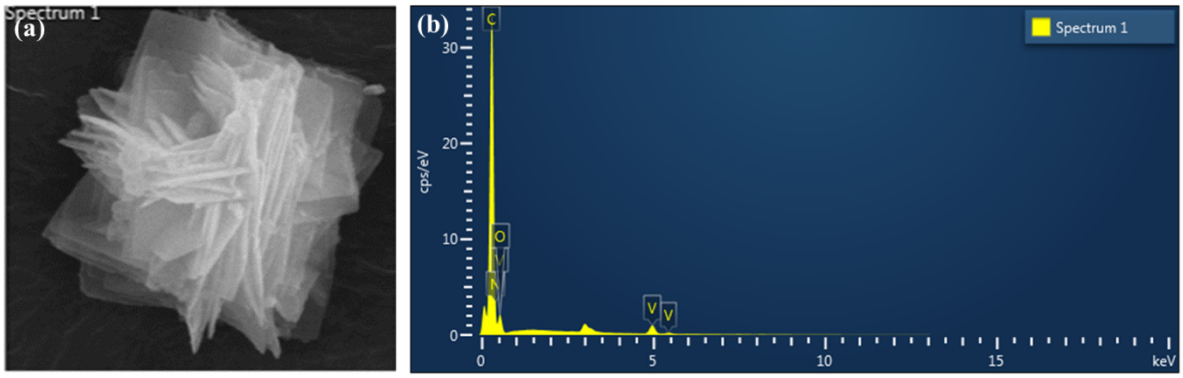

Element (c)	Line Type	Apparent Concentration	k Ratio	Wt%	Wt% Sigma	Atomic %	Standard Label	Factory Standard
C	K series	62.66	0.62660	78.59	0.30	84.06	C Vit	Yes
N	K series	0.00	0.00000	0.00	2.82	0.00	BN	Yes
O	K series	7.32	0.02463	19.13	0.31	15.36	SiO2	Yes
V	K series	1.90	0.01895	2.29	0.04	0.58	V	Yes
Total:				100.00		100.00		

Fig. S5. SEM EDX study. (a) Studied area V-MOF and corresponding; (b) EDX spectra; (c) Overall elemental composition table.

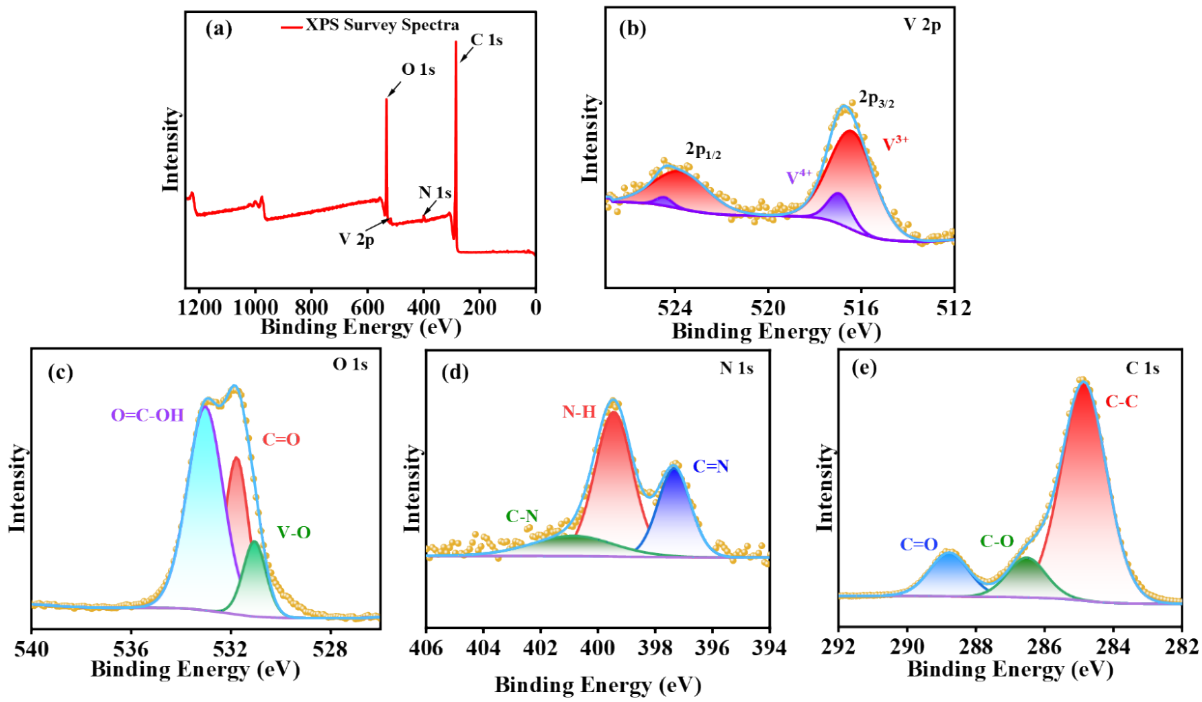

Fig. S6. (a) XPS survey spectrum of V-MOF (As synthesized); (b) High-resolution core-level V 2p XPS spectra in V-MOF, Core-level XPS spectra of (c) O 1s, (d) N 1s, and (e) C 1s.

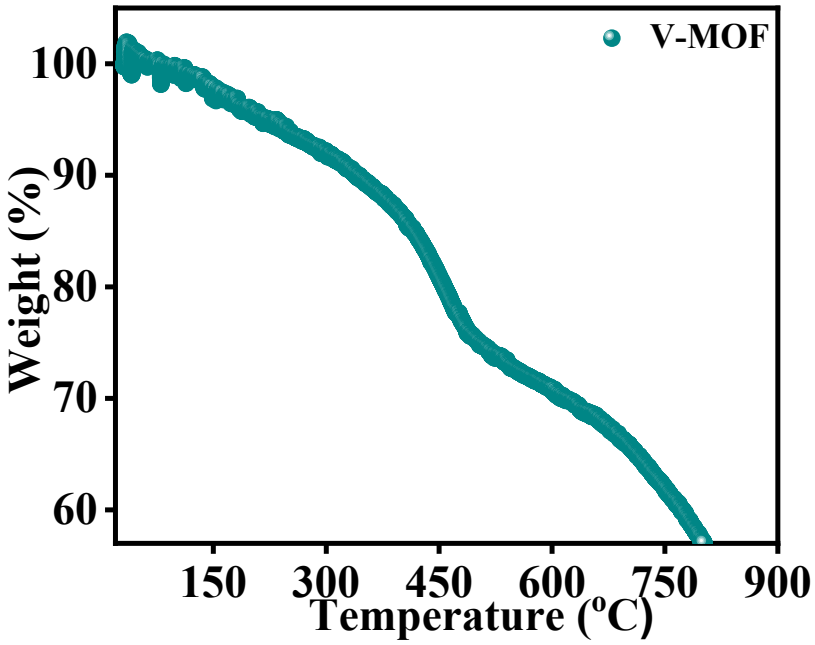

Fig. S7. The thermo-gravimetric (TG) analysis of the as-synthesised V-MOF.

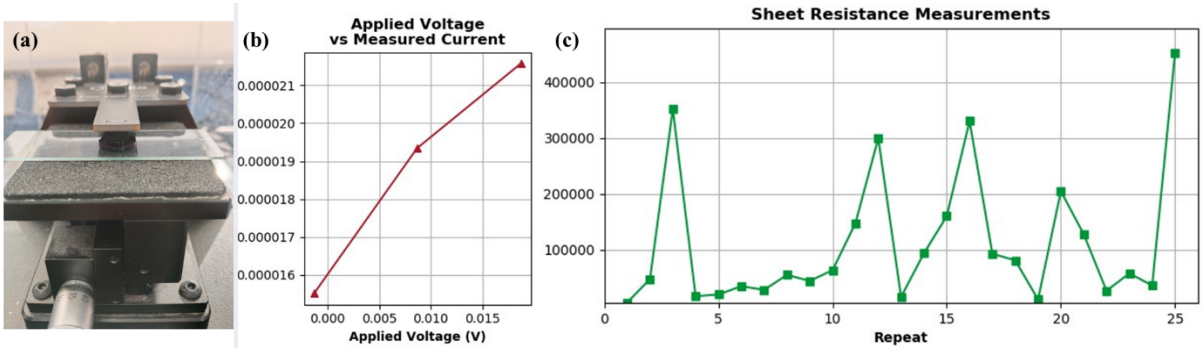

Fig. S8. (a) Presentations of the electrical conductivity measurement process; (b) Applied voltage vs current plot in V-MOF pellet using Ossila four-probe pellet instrument; (c) Sheet Resistance Measurement plot.

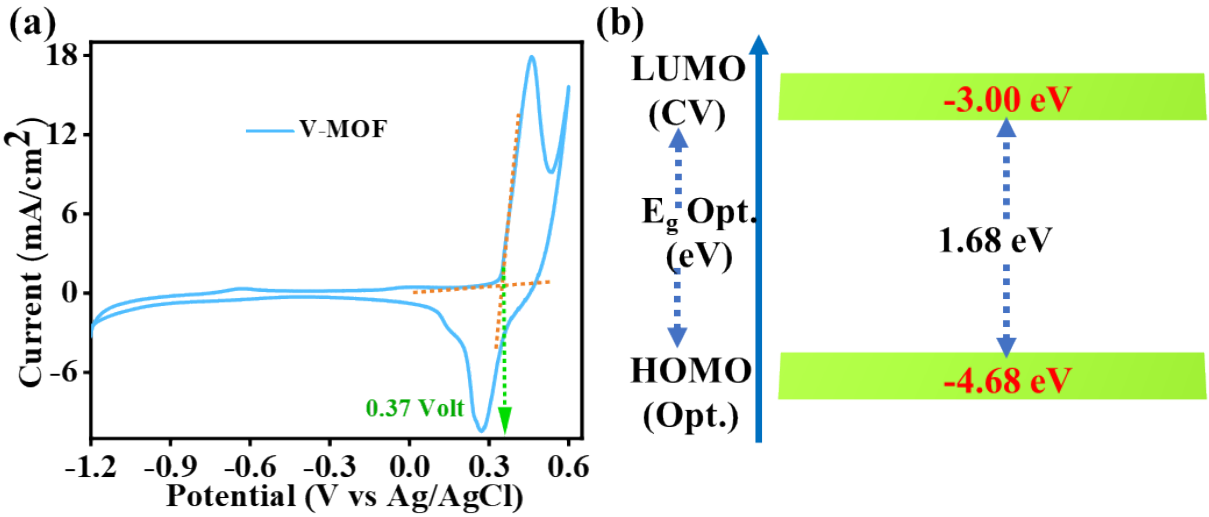

Fig. S9. (a) Cyclic Voltammogram. The HOMO and LUMO energy levels of V-MOF were calculated from the cyclic voltammogram, considering extreme oxidation and reduction onsets; (b) Approximate energy level of HOMO and LUMO in V-MOF.

Table S1. Comparison of the electrical conductivity of a few recent MOFs.

Materials	Conductivity (S cm^{-1})	Ref.	Dimensionality
Cu-TBC	6.8×10^{-4}(two-probe pellet)	*Chem. Commun.* **2023**, *59*, 2978.	2D
Cu-HAB	0.11 (four-contact pellet)	*Nat. Energy.* **2018***,* 3, 30.	2D
Ni-HAB	0.7 (four-contact pellet)		2D
Cu-HHB	7.3×10^{-8} (van der Pauw pellet)	*J. Am. Chem. Soc*. **2018**, *140,* 14533.	2D
Cu-HHTP	0.02 (two-probe film)	*Angew. Chem. Int. Ed.* **2017***, 56,* 16510.	2D
Ni-HHTP	0.01±0.003 (two-probe pellet)	*Chem. Mater.* **2016**, *28,* 5264.	2D
Cu-HHTQ	2.74×10^{-5} (two-probe pellet)	*Nano Res.* **2021**, *14,* 369.	2D
Cu-HITP	0.2 (two-point probe pellet)	*Angew. Chem. Int. Ed.* **2017**, *56,* 16510.	2D
$Fe_2(BDP)_3$	0.96	*Nat. Mater*. **2018**, *17*, 625−632.	3D
$Zn_2(SDC)_2(BPMTC)$	9.5×10^{-7}	*J. Am. Chem. Soc.* **2019**, *141*, 5350−5358.	3D
$Zn_2(BPDC)_2(BPMTC)$	6.4×10^{-7}		
$Fe_2(DOBDC)(DMF)_2$	3.2×10^{-7}	*J. Am. Chem. Soc.* **2015**, 137, 6164−6167.	3D
$Fe_2Cl_2(BTDD)$	1.1×10^{-7}	*Chem. Sci.* **2017**, 8, 4450−4457.	3D
Cu-$[Ni(PDT)_2]$	1.0×10^{-8}	*Chem. Mater.* **2010**, 22, 4120−4122.	3D
$Co_2(AnBHB)$	4.0×10^{-10}	*J. Am. Chem. Soc.* **2013,** 135, 8185−8188.	3D
Fe-MET	1.96×10^{-3} (four-probe pellet)	*Small*, **2024**, 20, 2401102.	3D
V-MOF	**1.762×10^{-3} (four-contact pellet)**	**This work**	

Thin Film Preparation:

The activated V-MOF sample (Kept overnight at 100 °C in a Vacuum Oven) electrode on pretreated Ni-foam was prepared for the electrochemical measurements. An EtOH: H_2O (4:1) solution mixture is taken to disperse the V-MOF (3 mg in 1 mL total volume with 10 µL Nafion as binder only) as active electrode materials were drop-cast (30 µL) on Ni-foam (1 cm × 1 cm) and dried in a vacuum oven at 100 ºC at overnight for further study as the working electrode.

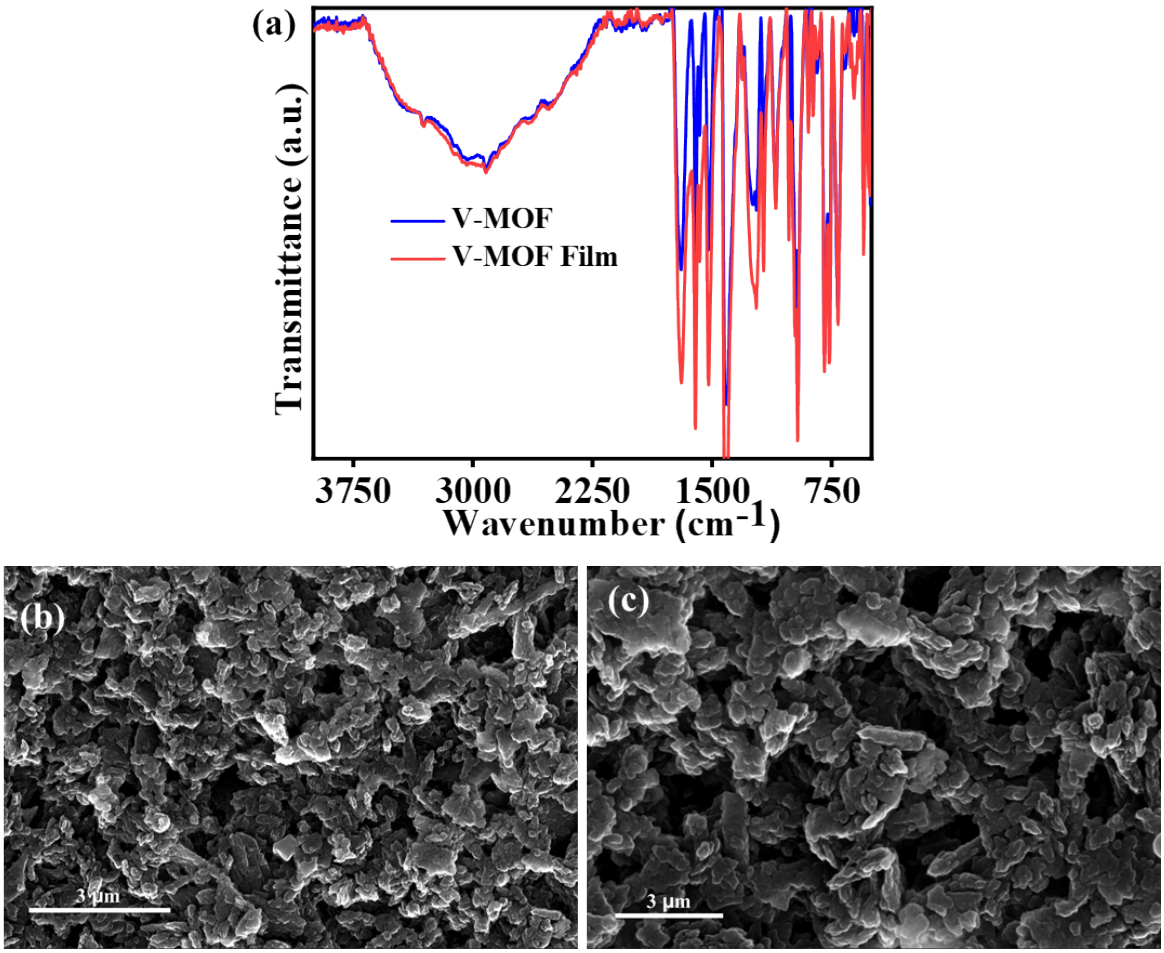

Fig. S10. Thin-film preparation on Ni-foam for three-electrode electrochemical studies. Characterisation of V-MOF thin film on Ni-foam through (a) FTIR, (b)-(c) FESEM.

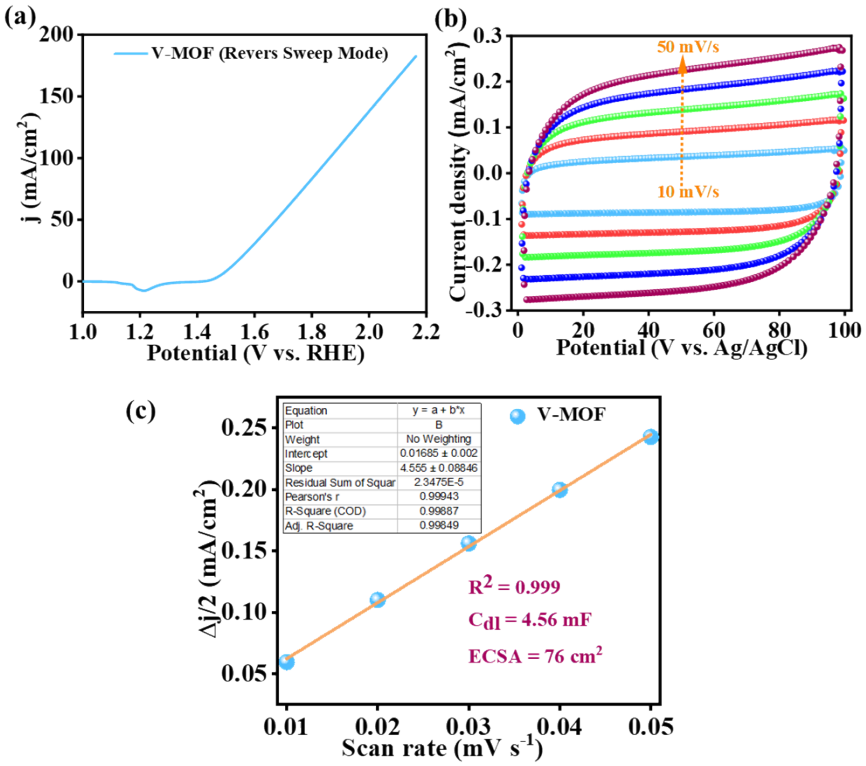

Fig. S11. (a) LSV of V-MOF modified electrode in reverse bias mode. (b) The CV curves were obtained in the non-Faradic region; (b) corresponding C_{dl} and ECSA calculation for V-MOF at different scan rates from 10 to 50 mV/s.

Table S2: Comparison of electrocatalytic OER activity of V-MOF with recently reported inorganic catalysts.

Electrocatalysts	**Synthesis method**	**Electrolyte KOH (M)**	**Overpotential (mV) @10mA/cm^2**	**Tafel slope (mV/dec)**	**Ref.**
$ZnCo_2O_4$ nanosheets with oxygen vacancies	Hydrothermal and NaBH4 reduction	0.1	324	56.9	S2
V-Co-Fe-343	hydrothermal	1	307	36.0	S3
$SmBa_{0.5}Sr_{0.5}Co_2O_{6-\delta}$ (SBSC-E(800))	hydrothermal	0.1	370	46.0	S4
ZnO@NiFe coreshell nanorods	electrodeposition	0.1	380	105	S5
$Co_{0.54}Fe_{0.46}(OOH)$	electrodeposition	1	370	26	S6
Au/NiFe LDH	hydrothermal	1	237	36	S7
$(Co,Ni)Se_2$@NiFeLDH	solvothermal	1	332	75	S8
Co_2P/Co_4N/CNTs	Pyrolysis	1	389	110	S9
PtNP-ZnO@CQDs	one-pot hydrothermal	1	355	61.7	S10
V-MOF	**solvothermal**	**1**	**260**	**56**	**This work**

Table S3: Comparison of electrocatalytic OER activity of V-MOF with other reported MOF-based catalysts.

Electrocatalyst	Metal ion	Ligand	Substrate	η_{10}	Tafel slope (mV/dec^{-1})	Ref.
Co-MOF	Co^{2+}	BDC	NF	311@50	54	S1
Ni-MOF	Ni^{2+}	BDC	NF	320@100	72	S12
Fe-MOF	Fe^{3+}	BDC	NF	240@50	72	S13
CoNi-MOFNA	Co^{2+}, Ni^{2+}	BDC	NF	215	51.6	S14
NiCo-MOF	Co^{2+}, Ni^{2+}	BDC	NF	270@50	35.4	S15
MIL-53(Co-Fe)	Fe^{3+}, Co^{2+}	BDC	NF	262@100	69	S16
NiFe-MOF	Fe^{3+}	BDC	NF	206.3	28.5	S17
NiFe-MOF	Ni^{2+}	BDC	IF	230	30.46	S18
NiFe-MOF	Ni^{2+}	BDC	IF	216@50	73.40	S19
FCN-MOF	Fe^{2+}, Co^{2+}, Ni^{2+}	BDC	NF	196	29.5	S20
MFN-MOF	Ni^{2+}, Fe^{3+}	BDC-NH_2	NF	235@50	55.4	S21
Fe-Ni MOF NSs	Fe^{3+}	BDC-NH_2	NF	258@50	40.8	S22
NiFe(20Ni)-MOF	Ni^{2+}	BDC-NH_2	NFF	226	87.1	S23
NiFe-MOF-74	Ni^{2+}, Fe^{2+}	H4DOBDC	NF	208	54	S24
FeMn-MOF	Fe^{3+}, Mn^{2+}	H4DOBDC	NF	290@50	87.02	S25
Co/Ni$(BDC)_2$TED	Co^{2+}, Ni^{2+}	BDC&TED	CF	260	76.24	S26
Ni-MOF	Ni^{2+}	BPDC	NF	350@20	98	S27
Co-MOF	Co^{2+}	BPDC	NF	290@20	74	S28
CoFe(dobpdc)-I	Co^{2+}, Fe^{2+}	Dobpdc	NF	197	52.00	S29
CoFe(dobpdc)-II				186	45.30	
CoFe(dobpdc)-III				176	35.10	
CoNi-MOF	Co^{2+}, Ni^{2+}	NDC	CF	265	56	S30
CoNi-NDC/PANI	Co^{2+}, Ni^{2+}	NDC	NF	323	73.3	S31
NiFe-MOF	Ni^{2+}, Fe^{3+}	NDC	NF	240	34	S32
NiMn-MOFs	Ni^{2+}, Mn^{2+}	NDC	MCCF	280	86	S33
Fe1Ni4-HHTP	Fe^{3+}, Ni^{2+}	HHTP	CC	213	96	S34
NiFc-MOF	Ni^{2+}	Fc	NF	195	44.1	S35
Fe-MIL-88A	Fe^{3+}	FA	NF	213@50	39.7	S36
Co-MOF NS	Co^{2+}	MIM	CC	320@20	104.9	S37
FeNi-MOF	Ni^{2+}, Fe^{2+}	TDC	NF	239@50	52.4	S38
FCN-MOF	Fe^{3+}, Co^{2+}, Ni^{2+}	BTC	NF	218	29.3	S39
V-MOF	**V^{3+}**	**H_6TCPP**	**NF**	**260**	**56**	**This Work**

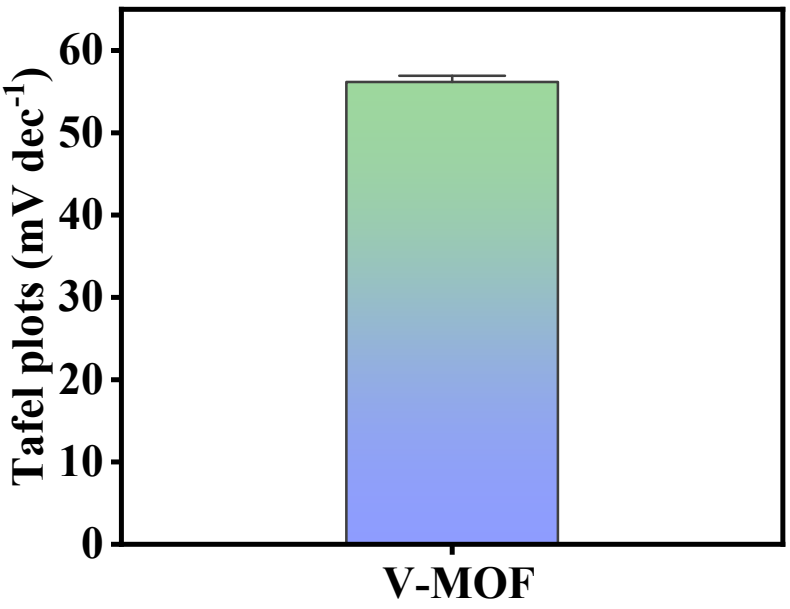

Fig. S12. The error-bar plot is used to determine the Standard Deviation (SD) for the Tafel Slope.

Proposed OER Catalytic Cycle for V-MOF (Alkaline Medium):

The discussion below illustrates the detailed mechanism and provides a clear view of the efficient OER activity of V-MOF. [S40-S42] Based on density functional theory (DFT) principles for metal-organic frameworks (MOFs) in the oxygen evolution reaction (OER) and the specific behaviour of vanadium-based materials, the catalytic cycle for V-MOF typically involves a four-electron mechanism in alkaline media. The V-nodes act as active sites, frequently undergoing surface reconstruction (e.g., to V-O or V-OH species) under operational potential.

$$\text{V-MOF} + OH^- \rightleftharpoons (\text{V-MOF})\text{-}OH^* + e^- \text{ (Adsorption of } OH^-\text{)}$$

$$(\text{V-MOF})\text{-}OH^* + OH^- \rightleftharpoons (\text{V-MOF})\text{-}O^* + H_2O + e^- \text{ (Deprotonation)}$$

$$(\text{V-MOF})\text{-}O^* + OH^- \rightleftharpoons (\text{V-MOF})\text{-}OOH^* + e^- \text{ (Hydroxyl attack)}$$

$$(\text{V-MOF})\text{-}OOH^* + OH^- \rightleftharpoons \text{V-MOF} + O_2 + H_2O + e^- \text{ (Oxygen evolution: Desorption)}$$

This catalytic cycle also influences vanadium's ability to adopt multiple oxidation states, facilitating the necessary electron transfer from (V-MOF)-OH* to (V-MOF)-OOH*.

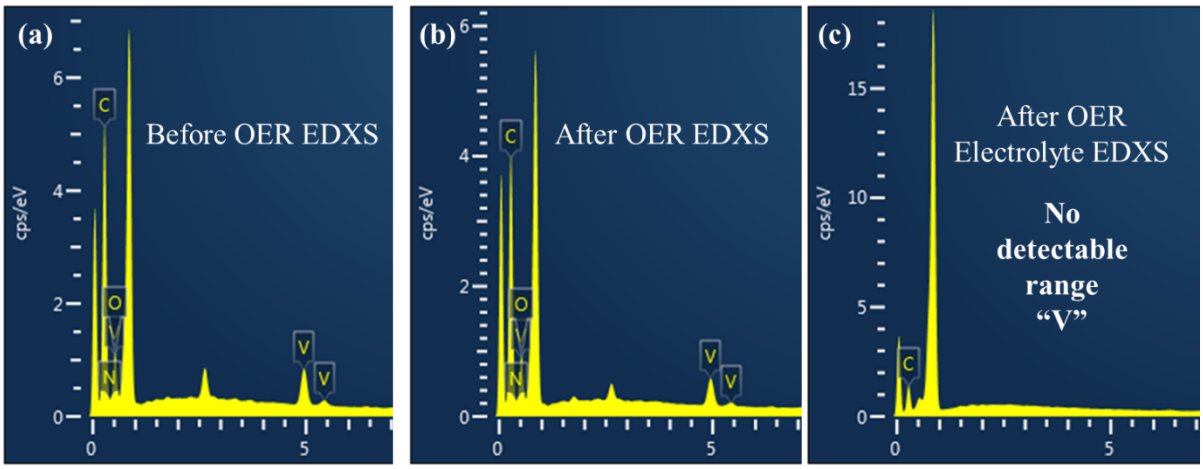

Fig. S13. (a-c) EDXS analysis supports the almost no leaching of vanadium during electrocatalysis, supporting the claim of durability of V-MOF.

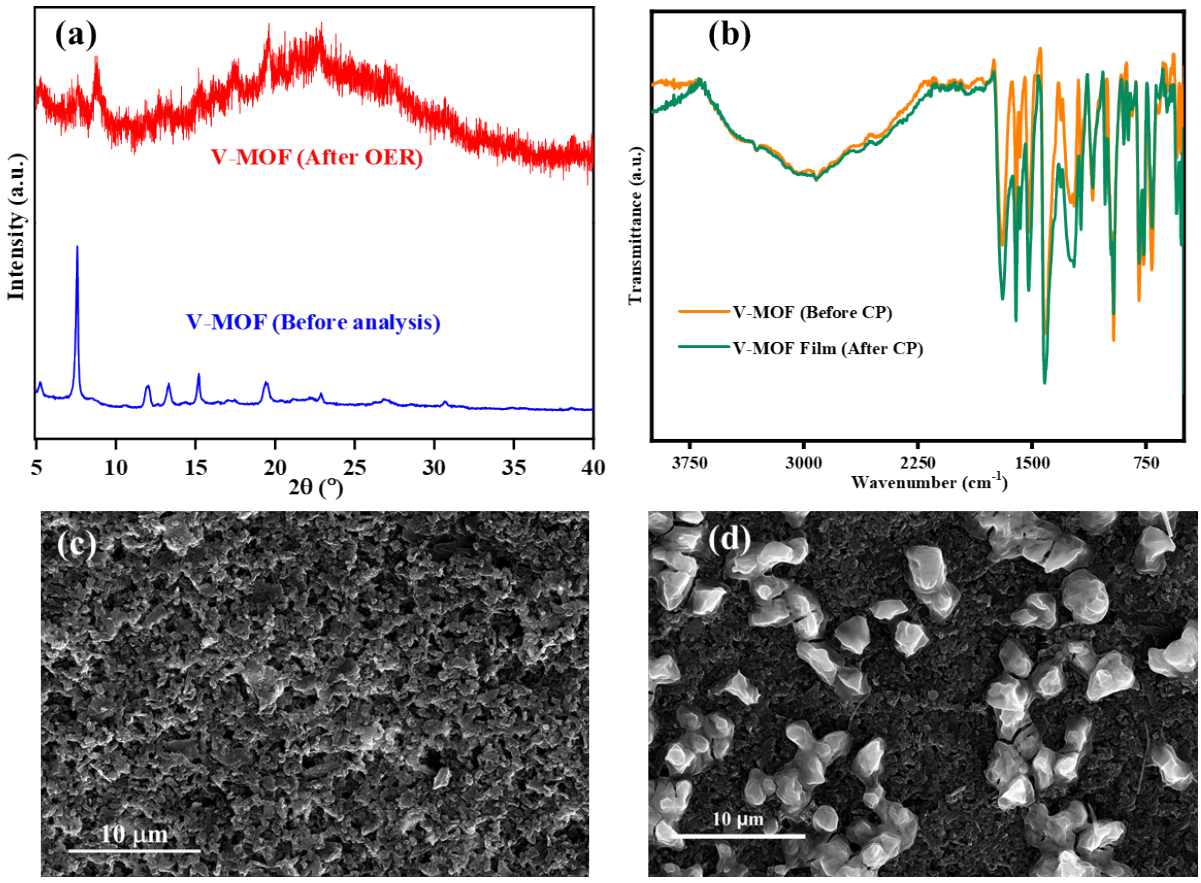

Fig. S14. (a) PXRD analysis of V-MOF before and after the analysis; (b) FTIR investigation of V-MOF before and after the chronopotentiometry; (c-d) FE-SEM study of V-MOF before and after the chronopotentiometry. The FESEM study of the V-MOF after OER suggests slight degradation of the nanosheet edges, which is corroborated by the ESCA analysis.

FWHM analysis of the V-MOF:

The FWHM analysis of the V-MOF before and after OER by using *Gaussian fitting*, and the particle sizes were also calculated by using the *Debye-Scherrer* equation: [S43-S45]

$$D = K\lambda/\beta COS\theta$$

D: Crystallite size (thickness).

K: Scherrer constant (~ 0.90)

λ: X-ray wavelength.

β: FWHM in radians (peak broadening).

θ: Bragg angle.

From the calculations, we found slight decreases in the crystalline sizes of V-MOF, and a minor amorphization effect was observed after the OER process.

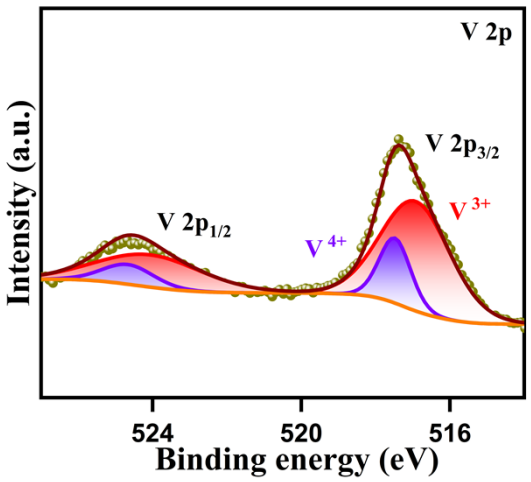

Fig. S15. The XPS spectra of V after OER.

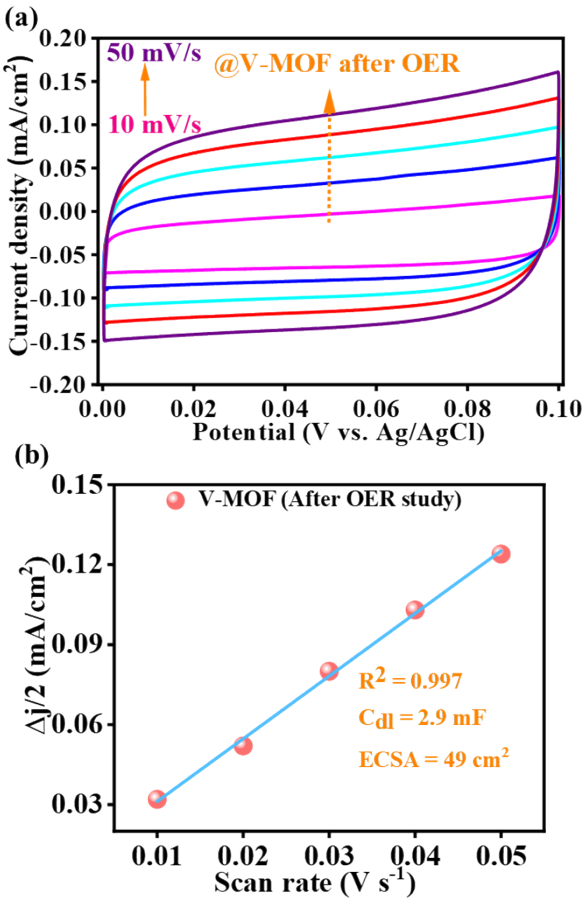

Fig. S16. (a) The CV curves, in the non-Faradic region; (b) corresponding C_{dl} and ECSA calculation for V-MOF at different scan rates from 10 to 50 mV/s (After OER analysis).

Supporting References:

[S1]. M. V. Nguyen, H. C. Dong, V. T. Truong, H. N. Nguyen, L. C. Luu, N. N. Dang and T. A. Nguyen, *New J. Chem.*, 2022, **46**, 632–641.

[S2]. K. Xiang, D. Wu, Y. Fan, W. You, D. Zhang, J.-L. Luo and X.-Z. Fu, *Chem. Eng. J.*, 2021, **425**, 130583.

[S3]. T. Gao, Z. Jin, M. Liao, J. Xiao, H. Yuan and D. Xiao, *J. Mater. Chem. A*, 2015, **3**, 17763-17770.

[S4]. H. Zhang, D. Guan, X. Gao, J. Yu, G. Chen, W. Zhou and Z. Shao, *J. Mater. Chem. A*, 2019, **7**, 19228-19233.

[S5]. Z. Zhao, H. Wu, H. He, X. Xu and Y. Jin, J. Mater. Chem. A, 2015, 3, 7179-7186.

[S6]. M.-S. Burke, M.-G. Kast, L. Trotochaud, A.-M. Smith and S.-W. Boettcher, *J. Am. Chem. Soc.*, 2015, **137**, 3638-3648.

[S7]. J. Zhang, J. Liu, L. Xi, Y. Yu, N. Chen, S. Sun, W. Wang, K.-M. Lange and B. Zhang, *J. Am. Chem. Soc.*, 2018, **140**, 3876-3879.

[S8]. J.-G. Li, H. Sun, L. Lv, Z. Li, X. Ao, C. Xu, Y. Li and C. Wang, *ACS Appl. Mater. Interfaces*, 2019, **11**, 8106-8114.

[S9]. Z. Cai, L. Xu, Y. Zhou, L. Gao, X. An, X. Ma, Y. Ma, J. Liu, X. Li and K. Tang, Int. *J. Hydrogen Energy*, 2024, **82**, 559-566.

[S10]. A. K. Pradhan, S. Halder and C. Chakraborty, *J. Mater. Chem. A*, 2025, **13**, 243-256.

[S11]. X. Zhang, W. Sun, H. Du, R.-M. Kong and F. Qu, *Inorg. Chem. Front.*, 2018, **5**, 344–347.

[S12]. Q. Liu, L. Xie, X. Shi, G. Du, A. M. Asiri, Y. Luo and X. Sun, *Inorg. Chem. Front.*, 2018, **5**, 1570–1574.

[S13]. X. Zhang, Q. Liu, X. Shi, A. M. Asiri and X. Sun, *Inorg. Chem. Front.*, 2018, **5**, 1405–1408.

[S14]. L. Huang, G. Gao, H. Zhang, J. Chen, Y. Fang and S. Dong, *Nano Energy*, 2020, **68**, 104296.

[S15]. P. Thangasamy, S. Shanmuganathan and V. Subramanian, *Nanoscale Adv.*, 2020, **2**, 2073–2079.

[S16]. M. Xie, Y. Ma, D. Lin, C. Xu, F. Xie and W. Zeng, *Nanoscale*, 2020, **12**, 67–71.

[S17]. F.-X. Ma, F. Lyu, Y. Diao, B. Zhou, J. Wu, F. Kang, Z. Li, X. Xiao, P. Wang, J. Lu and Y. Y. Li, *Nano Res.*, 2022, **15**, 2887–2894.

[S18]. Y. Zhang, J. Wang, L. Ye, M. Zhang and Y. Gong, *Dalton Trans.*, 2021, **50**, 4720–4726.

[S19]. Y. Jia, Z. Xu, L. Li and S. Lin, *Dalton Trans.*, 2022, **51**, 5053–5060.

[S20]. D. Senthil Raja, C.-L. Huang, Y.-A. Chen, Y. Choi and S.-Y. Lu, *Appl. Catal., B*, 2020, **279**, 119375.

[S21]. D. Senthil Raja, H.-W. Lin and S.-Y. Lu, *Nano Energy*, 2019, **57**, 1–13.

[S22]. C. Pan, Z. Liu and M. Huang, *Appl. Surf. Sci.*, 2020, **529**, 147201.

[S23]. J. Wang, Y. Jiang, C. Liu, Y. Wu, B. Liu, W. Jiang, H. Li and G. Che, *J. Colloid Interface Sci.*, 2022, **614**, 532–537.

[S24]. C. Chen, N. Suo, X. Han, X. He, Z. Dou, Z. Lin and L. Cui, *J. Alloys Compd.*, 2021, **865**, 158795.

[S25]. H. Guan, N. Wang, X. Feng, S. Bian, W. Li and Y. Chen, *Colloids Surf., A*, 2021, **624**, 126596.

[S26]. D.-J. Li, Q.-H. Li, Z.-G. Gu and J. Zhang, *J. Mater. Chem. A*, 2019, **7**, 18519–18528.

[S27]. C. Meng, Y. Cao, Y. Luo, F. Zhang, Q. Kong, A. A. Alshehri, K. A. Alzahrani, T. Li, Q. Liu and X. Sun, *Inorg. Chem. Front.*, 2021, **8**, 3007–3011.

[S28]. J. Yu, Y. Cao, Q. Liu, Y. Luo, Y. Liu, X. Shi, A. M. Asiri, T. Li and X. Sun, *ChemNanoMat*, 2021, **7**, 906–909.

[S29]. Z. Xu, C. L. Yeh, Y. Jiang, X. Yun, C. T. Li, K. C. Ho, J. T. Lin and R. Y. Lin, *ACS Appl. Mater. Interfaces*, 2021, **13**, 28242–28251.

[S30]. M. Liu, W. Zheng, S. Ran, S. T. Boles and L. Y. S. Lee, *Adv. Mater. Interfaces*, 2018, **5**, 1800849.

[S31]. W.-J. Dang, Y.-Q. Shen, M. Lin, H. Jiao, L. Xu and Z.-L. Wang, *J. Alloys Compd.*, 2019, **792**, 69–76.

[S32]. J. Duan, S. Chen and C. Zhao, *Nat. Commun.*, 2017, **8**, 15341.

[S33]. W. Cheng, X. F. Lu, D. Luan and X. W. D. Lou, *Angew. Chem., Int. Ed.*, 2020, **59**, 18234–18239.

[S34]. W.-H. Li, J. Lv, Q. Li, J. Xie, N. Ogiwara, Y. Huang, H. Jiang, H. Kitagawa, G. Xu and Y. Wang, *J. Mater. Chem. A*, 2019, **7**, 10431–10438.

[S35]. J. Liang, X. Gao, B. Guo, Y. Ding, J. Yan, Z. Guo, E. C. M. Tse and J. Liu, *Angew. Chem., Int. Ed.*, 2021, **60**, 12770–12774.

[S36]. M. Ying, R. Tang, W. Yang, W. Liang, G. Yang, H. Pan, X. Liao and J. Huang, *ACS Appl. Nano Mater.*, 2021, **4**, 1967–1975.

[S37]. Z. Wei, W. Zhu, Y. Li, Y. Ma, J. Wang, N. Hu, Y. Suo and J. Wang, *Inorg. Chem.*, 2018, **57**, 8422–8428.

[S38]. C.-P. Wang, Y. Feng, H. Sun, Y. Wang, J. Yin, Z. Yao, X.-H. Bu and J. Zhu, *ACS Catal.*, 2021, **11**, 7132–7143.

[S39]. Z. Li, S. Deng, H. Yu, Z. Yin, S. Qi, L. Yang, J. Lv, Z. Sun and M. Zhang, *J. Mater. Chem. A*, 2022, **10**, 4230–4241.

[S40]. F. Wu, K. Ye and J. Jiang, *J. Phys. Chem. Lett.*, 2025, **16**, 7780-7788.

[S41]. Z. Wang, M. Liu, Z. Tan, Y. Wang, Y. Liang, B. Liang, Y. Hu, Y. Yang, C. Duan, K. Qi and H. Xi, *Nano Mater. Sci.*, 2026.

[S42]. H. Li, J. Wu, M. Li and Y. Wang, Catalysts, 2024, 14, 368.

[S43]. U. Holzwarth and N. Gibson, *Nat. Nanotechnol.*, 2011, **6**, 534.

[S44]. M. A. R. Miranda and J. M. Sasaki, *Acta Crystallogr., Sect. A: Found. Crystallogr.*, 2018, **74**, 54-65.

[S45]. A. W. Burton, K. Ong, T. Rea and I. Y. Chan, *Microporous Mesoporous Mater.*, 2009, **117**, 75-90.